Supporting Information

Zhuravlev et al. 10.1073/pnas.1200160109

SI Text

Efficiency of Active Transport and Nonmonotonic Profile. As mentioned in the main text, the maximum in the actin profile is pumped up by the motors, and should gradually disappear if the transport becomes less and less efficient. The actin profiles for different values of the loading rate, k_l, (binding between a motor on filament and a G-actin monomer) are plotted in Fig. S1, clearly illustrating this effect.

The Boundary Conditions. The choice of the third boundary condition (BC) for the equations describing the motor profiles is a subtle issue and depends on the particular question one has in mind. This choice only has a slight effect on the solution of the equations, so it is not very important. However, it is worthwhile to discuss it for clarity purposes.

For the purely mathematical, continuous problem, where the filaments do not exist outside the tube, the appropriate boundary condition is $c_b(0) = 0$ [from which follows the $A(0) = 0$ in the actin part] and no additional assumptions (like detailed balance) are required. Indeed, if the filaments do not cross the $z = 0$ point, neither can bound motors, hence $J_b(0) = 0$, and as $J_b = v(c_b)c_b$, $c_b(0) = 0$. This argument can be presented in a more detailed way. Let us consider a small (going to infinitesimal later) volume of the tube near the base. Integrating the second of the motor equations over this volume, one gets

$$\frac{\partial J_b}{\partial z} = -k_{\text{off}}c_b + k_{\text{on}}c_f, \qquad \textbf{[S1]}$$

$$\int_0^{\delta z} \frac{\partial J_b}{\partial z} dxdydz = \int_0^{\delta z} (-k_{\text{off}}c_b + k_{\text{on}}c_f) dxdydz, \qquad \textbf{[S2]}$$

$$[J_b(0 + \delta z) - J_b(0+)]S_f = [-k_{\text{off}}c_b(\alpha\delta z) + k_{\text{on}}c_f(\alpha\delta z)]S_f\delta z, \qquad \textbf{[S3]}$$

where S_f is cross-section of the filopodium and $0 \le \alpha \le 1$.

Because $J_b(0+) = 0$,

$$J_b(0 + \delta z)S_f = [-k_{\text{off}}c_b(\alpha\delta z) + k_{\text{on}}c_f(\alpha\delta z)]S_f\delta z, \qquad \textbf{[S4]}$$

$$\lim_{\delta z\to 0} J_b(\delta z) = \lim_{\delta z\to 0}[-k_{\text{off}}c_b(\alpha\delta z) + k_{\text{on}}c_f(\alpha\delta z)]\delta z = 0, \qquad \textbf{[S5]}$$

and as $J_b = v(c_b)c_b$, one can conclude that $\lim_{\delta z\to 0} c_b(\delta z) = 0$ and use the boundary condition

$$c_b(0) = 0. \qquad \textbf{[S6]}$$

In our simulations, however, the space is split into compartments, the concentration profiles are not continuous, and the first point corresponds to the first compartment, which spans 54 nm starting from $z = 0$. It is not obvious how to directly compare the simulation results with continuous analytical curves at $z = 0$. To compare, one should take the average of the analytical curve over the first 54 nm and using it as $c_b(0)$ and solve the equations again. Alternatively, one can assume detailed balance between c_f and c_b at $z = 0$ (and between c_b and A in the actin equations), which turns out to be a good approximation.

In real filopodia the filaments continue into the cell bulk (unlike our simulations), making the $c_b = 0$ condition of the formal problem less relevant. Detailed balance in the cell bulk, on the other hand, is a plausible assumption as a first approximation. The next approximation would require modeling of the filaments with motors in the bulk (the lamellipodium) explicitly.

Thus, the detailed balance BCs are more interesting and relevant for the physical problem, so they are the ones used in the paper. However, it turns out that both alternative BCs lead to almost indistinguishable results, except for the very beginning of the concentration profiles. To demonstrate this indistinguishability, we plotted below the graphs corresponding to the solution of the formal mathematical problem, with no additional assumptions, and the $c_b(0) = 0$ boundary condition (Figs. S4–S8).

Weak Detailed Balance Violation in the Motor Part. Let us introduce the extent of the detailed balance violation between motor binding to the filaments and falling off as a variable, δj_u:

$$k_{\text{off}}c_b = k_{\text{on}}(1 - c_b/c_s)c_f + \delta j_u \qquad \textbf{[S7]}$$

for all z, where $\delta j_u(z)$ is the deviation from the detailed balance in the form of unbinding motor current density. The jammed motor model (JMM) equations become rewritten as

$$\begin{cases} -Dc_f''(z) = \delta j_u(z), \\ [c_b(z)[v(1 - c_b(z)/c_s] - v_r)]' = -\delta j_u(z). \end{cases} \qquad \textbf{[S8]}$$

The detailed balance violation is what drives the system and creates the motor profiles. Essentially, the violation is proportional to the active transport intensity, as one can see from the second equation. It creates cyclic currents in the tube with motors binding to the filaments, actively going forward, falling off, and diffusing backward, as illustrated on Fig. S2. However, it is interesting that, with the $c_b(0) = 0$ boundary condition, the detailed balance near the base, or something very close to it, is approached very fast. Plotting the deviation $\delta j_u(z)$ in Fig. S3, we see that, apart from narrow region near the base, it is small compared to either one of the binding or unbinding flux densities. In other words, the detailed balance along the whole tube is only violated weakly, or $\delta j_u \ll k_{\text{off}}c_b \sim k_{\text{on}}(1 - c_b/c_s)c_f$. Nevertheless, we cannot set $\delta j_u(z) \equiv 0$, despite it being small, as it is the essential part of the dynamical system described by the JMM. Obviously, assuming full detailed balance would trivialize both JMM equations, leading to flat, or, at most linear concentration profiles. However, we can use conservation law for the total flux (which comes from summing the equations, so that δj_u cancels, see main text), $J_b + J_f = 0$, or

$$-Dc_f' + c_b[v(1 - c_b/c_s) - v_r] = 0, \qquad \textbf{[S9]}$$

along with Eq. **S7** to substitute c_b, and the fact that $\delta j_u(z)$ is small:

$$c_b = \frac{k_{\text{on}}c_f - \delta j_u}{k_{\text{off}} + k_{\text{on}}c_f/c_s} \approx \frac{k_{\text{on}}c_f c_s}{k_{\text{off}}c_s + k_{\text{on}}c_f}. \qquad \textbf{[S10]}$$

Substituting this relation into the conservation law, we obtain a single equation for c_f:

$$c_f' = \frac{1}{D}\frac{k_{\text{on}}c_f c_s}{k_{\text{off}}c_s + k_{\text{on}}c_f}\left[v\left(1 - \frac{k_{\text{on}}c_f}{k_{\text{off}}c_s + k_{\text{on}}c_f}\right) - v_r\right]. \qquad \textbf{[S11]}$$

Using notation $f = k_{\text{on}}c_f/k_{\text{off}}c_s$, $\gamma = (v - v_r)/v_r$, we rewrite the equation as

$$f' = \frac{k_{on} v_r}{k_{off} D} \frac{\gamma f - f^2}{(1+f)^2}. \quad \textbf{[S12]}$$

The variables are separated so we can directly integrate the equation

$$z + C = \frac{k_{off} D}{k_{on} v_r \gamma} (\log f - (1+\gamma)^2 \log|f-\gamma| - \gamma f). \quad \textbf{[S13]}$$

Taking into account the boundary condition

$$f(z)|_{z=0} = f_0 = \frac{k_{on} c_f(0)}{k_{off} c_s}, \quad \textbf{[S14]}$$

we obtain the solution

$$z = \frac{k_{off} D}{k_{on} v_r} \left(\frac{1}{\gamma} \log \left[\frac{f}{f_0} \left(\frac{f_0 - \gamma}{f - \gamma} \right)^{(1+\gamma)^2} \right] + f_0 - f \right). \quad \textbf{[S15]}$$

Alternatively, one can substitute c_f as a function of c_b, yielding a different equation, which looks more complicated and also requires $\delta j_u'(z)$ to be small as well (in our case, it is):

$$c_f = \frac{k_{off}}{k_{on}} \frac{c_b - \delta j_u / k_{off}}{1 - c_b/c_s} \approx \frac{k_{off}}{k_{on}} \frac{c_b}{1 - c_b/c_s}, \quad \textbf{[S16]}$$

$$c_f' \approx \frac{k_{off}}{k_{on}} \frac{c_b' - \delta j_u' / k_{off}(1 - c_b/c_s)}{(1 - c_b/c_s)^2}, \quad \textbf{[S17]}$$

where terms with δj_u are already dropped. If the derivative of the deviation is also small, i.e.,

$$\delta j_u' \ll k_{on} c_f' (1 - c_b/c_s) \sim k_{off} c_b' / (1 - c_b/c_s), \quad \textbf{[S18]}$$

we can write down a single equation for c_b:

$$c_b' = \frac{k_{on}}{k_{off} D} c_b (1 - c_b/c_s)^2 [v(1 - c_b/c_s) - v_r], \quad \textbf{[S19]}$$

or

$$b' = \frac{k_{on} v}{k_{off} D} b (1-b)^2 (1 - b - r), \quad \textbf{[S20]}$$

where $b = c_b/c_s$, $r = v_r/v$. The solution is

$$z + C = \frac{k_{off} D}{k_{on} v_r} \left[\frac{\log \frac{b'^2 (1-b)^{(1-r^2)}}{|1-r-b|}}{r(1-r)} - \frac{1}{1-b} \right]. \quad \textbf{[S21]}$$

Like before, C is just the same expression with $z = 0$ and $b(0) = b_0 = c_b(0)/c_s = k_{on} c_f(0) / [k_{off} c_s + k_{on} c_f(0)]$:

$$z = \frac{k_{off} D}{k_{on} v_r} \left[\frac{\log \left[\left(\frac{b(1-b_0)}{b_0(1-b)} \right)^{r^2} \frac{(1-b)|1-r-b_0|}{(1-b_0)|1-r-b|} \right]}{r(1-r)} - \frac{b - b_0}{(1-b)(1-b_0)} \right]. \quad \textbf{[S22]}$$

Eqs. **S15** and **S22** give identical results for our parameters, as one should expect, but the former has no additional requirement of slow change of detailed balance deviation in space and has a simpler expression, so we included it in the main text.

It is possible to perform a similar approximation for the actin part of the problem, as there the detailed balance between G-actin loading and unloading onto the motors seems to also be violated weakly. However, $c_b(z)$ enters the into the actin equations and prevents the variables from being separated [even if we had an explicit expression for $c_b(z)$ rather than $z(c_b)$], so there does not seem to be simple way of obtaining analytical solution for the actin part.

G-Actin Profiles and Experiments. Although motor profiles within our model are universal (independent of length), G-actin profiles will obviously be different for different lengths. In fact, G-actin profile sets up the stationary length. However, at stationary length, they will have common features (provided there is no special mechanisms additional to those we consider in this work): negative slopes at the base and at the tip, concentration at the tip such that polymerization balances the retrograde flow. The (de)polymerization rates k^+ and k^- depend on the membrane stress, which can depend on the length, adding a correction to the Eq. **5** in the main text. However, to the first approximation of the straight tube, the membrane force does not depend on the length (1).

Experimental observation of G-actin profiles in filopodia is complicated, mainly because of the presence of large amounts of F actin. There are techniques to discriminate between the two, like labeling only a small fraction of actin or labeling DNase I, which only binds to G actin but not F actin (2). Hopefully, the latter can achieve sufficient spatial resolution for obtaining the profiles in the narrow tube full of F actin like a filopodium or a stereocilium.

More Connections to Experiments. Apart from the decrease in the effective motor speed due to traffic jamming, the ATP hydrolysis rate itself (by an individual motor) can decrease due to autophosphorylation, as the local motor concentration increases (3, 4).

There is no direct experimental evidence of G-actin monomers being transported by either Myosin III or Myosin X, but these motors do carry espin1 and enabled/vasodilator-stimulated phosphoprotein (Ena/VASP), respectively. Both espin1 and Ena/VASP have actin-binding domains, which prompts a plausible suggestion that they may be serving as "delivery devices," adaptors, or scaffolds, between the motor and G actin. We investigated this possibility in our previous work on active transport in filopodia, for Ena/VASP and Myosin X (the framework is general, however, and equally applies to espin1 and Myosin IIIa) (5). Presence of espin1 promotes elongation of the filopodia (3, 6), although it may be due to its anticapping and polymerization-promoting functionality rather than active G-actin delivery. Ena/VASP is known to have an anticapping role.

Retrograde Flow. The retrograde flow plays an important role in setting up the stationary length because it defines the actin flux through the filopodial cross-section (or, rather two equal fluxes with opposite signs). In the model reported in this work, we use a constant retrograde flow speed, which depends neither on polymerization nor on various protein concentrations. In reality, the retrograde flow rate can be influenced by many factors both in the cell bulk (active machinery pulling filaments back; rearrangements and filament degradation in lamellipodia) or in filopodia itself, like focal adhesions (7), or force from the membrane acting on a filament which is polymerizing against it. We investigated the coupling between the retrograde flow and polymerization in our previous work (reported in the supplemental information of ref. 5). This coupling can be easily taken into account in the mean-field sense, where the results are in close agreement with more detailed stochastic simulations that allow for the retrograde flow fluctuations. In this work, we focused on the phenomena brought in by molecular motors inside the filopodium and, hence, chose in favor of a simpler model where the retrograde flow is simply held constant and does not depend on other parameters and processes. This assumption can be released in a straightforward manner, if needed.

1. Atilgan E, Wirtz D, Sun SX (2006) Mechanics and dynamics of actin-driven thin membrane protrusions. *Biophys J* 90:65–76.
2. Cramer LP, Briggs LJ, Dawe HR (2002) Use of fluorescently labelled deoxyribonuclease I to spatially measure G actin levels in migrating and non-migrating cells. *Cell Motil Cytoskeleton* 51:27–38.
3. Salles FT, et al. (2009) Myosin IIIa boosts elongation of stereocilia by transporting espin 1 to the plus ends of actin filaments. *Nature Cell Biol* 11:443–450.
4. Quintero OA, et al. (2010) Intermolecular autophosphorylation regulates myosin IIIa activity and localization in parallel actin bundles. *J Biol Chem* 285:35770–35782.
5. Zhuravlev PI, Der BS, Papoian GA (2010) Design of active transport must be highly intricate: A possible role of myosin and Ena/VASP for G actin transport in filopodia. *Biophys J* 98:1439–1448.
6. Merritt RC, et al. (2012) Myosin IIIB uses an actin-binding motif in its espin-1 cargo to reach the tips of actin protrusions. *Curr Biol* 22:320–325.
7. Chan CE, Odde DJ (2008) Traction dynamics of filopodia on compliant substrates. *Science* 322:1687–1691.

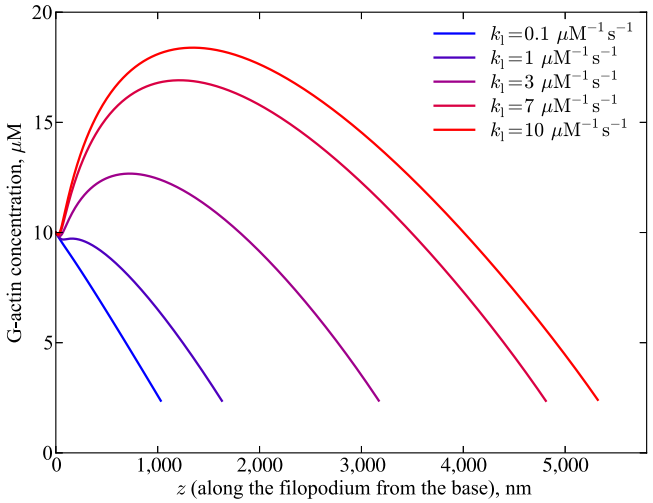

Fig. S1. One of the possible ways to influence the efficiency of transport is to change binding rate of G actin to motors. Concentration profile changes to a monotonic when transport becomes completely inefficient.

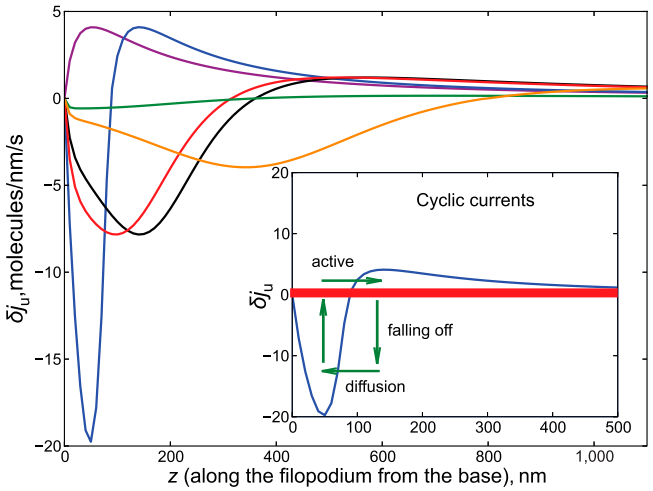

Fig. S2. The difference between the binding and unbinding flux densities along the tube is shown. The inset illustrates cyclic currents created by violated detailed balance. The red bar represents the actin filaments. Close to the base, there is a negative minimum in δj_u (binding flux is greater than unbinding), so there is net binding current, which is then translated into active transport flux forward (which has a maximum at the same point), and then, after the traffic jam is built up, net binding changes to net unbinding, which is translated to diffusion backward.

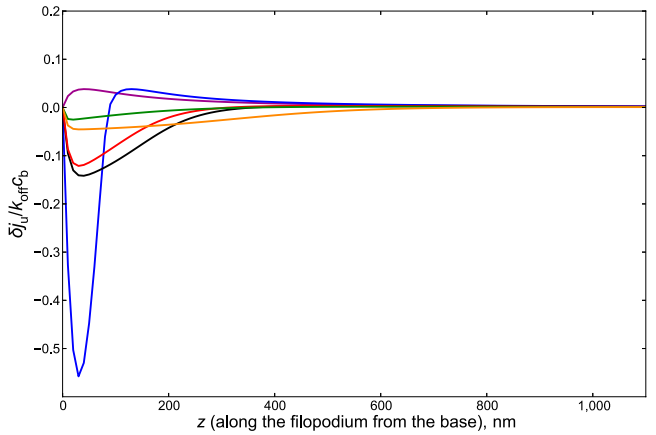

Fig. S3. Unbinding and binding flux density difference (deviation from detailed balance) in relation to the unbinding flux density is shown to illustrate the former is small compared to the latter everywhere in the tube except near the very base.

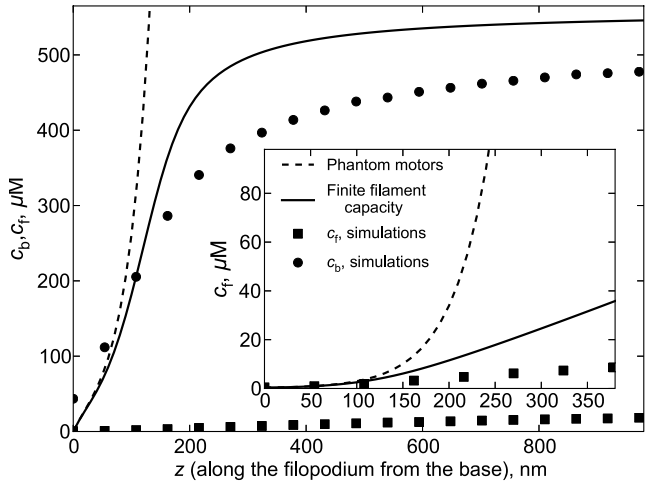

Fig. S4. Comparison of the mean-field analytical models with the stochastic simulation results for the $c_b(0) = 0$ boundary condition.

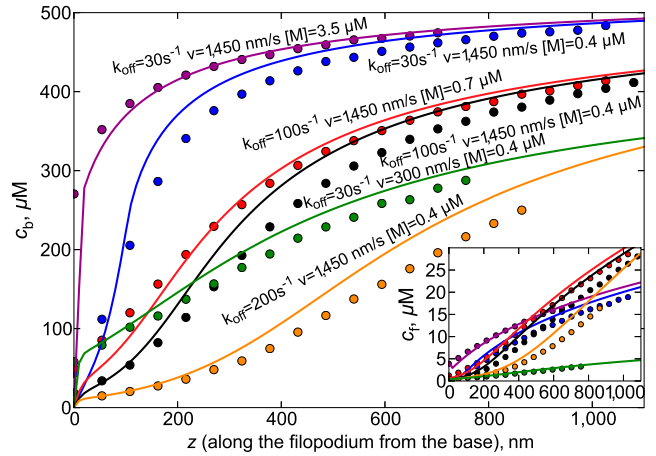

Fig. S5. Motor concentration profiles inside a filopodium according to stochastic simulations and jammed motors model for various parameter sets (motor affinity to filaments, motor speed, motor concentration). Inset zooms into low-concentration region to show curves for c_f. The figure corresponds to the $c_b(0) = 0$ boundary condition.

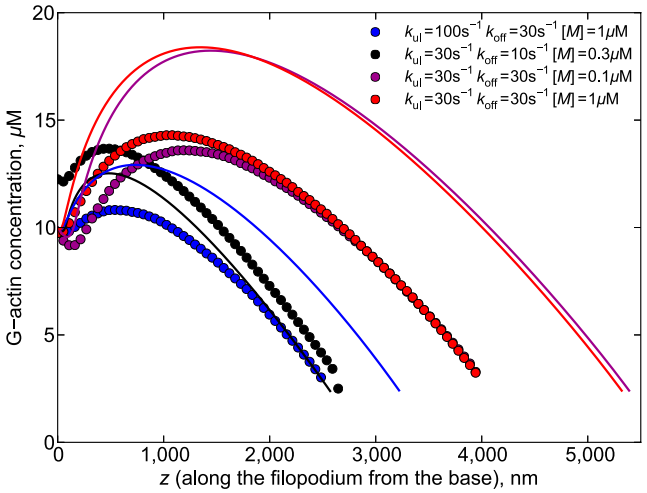

Fig. S6. G-actin concentration profiles for different parameter values are shown, for the $c_b(0) = 0$, $A(0) = 0$ boundary conditions.

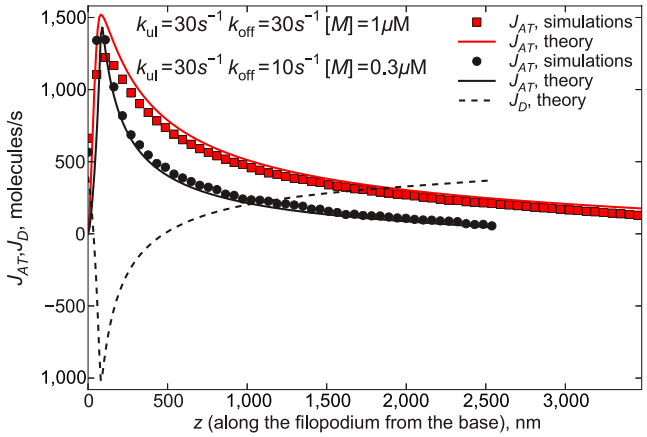

Fig. S7. Active transport and diffusional fluxes for the $c_b(0) = 0$, $A(0) = 0$ boundary conditions are shown.

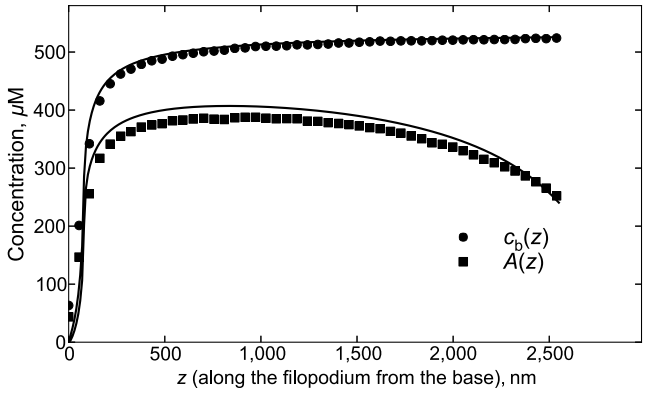

Fig. S8. Concentration profiles for actin-on-the-motors $A(z)$ and motors $c_b(z)$ are shown for $k_{ul} = 30\ s^{-1}$, $k_{off} = 10\ s^{-1}$, [M] = 0.3 μM for the $c_b(0) = 0$, $A(0) = 0$ boundary conditions.